Endothelial GqPCR activity controls capillary electrical signaling and brain blood flow through PIP$_2$ depletion

Osama F. Harraz[a], Thomas A. Longden[a], Fabrice Dabertrand[a], David Hill-Eubanks[a], and Mark T. Nelson[a,b,1]

[a]Department of Pharmacology, College of Medicine, University of Vermont, Burlington, VT 05405; and [b]Institute of Cardiovascular Sciences, University of Manchester, M13 9PL Manchester, United Kingdom

Brain capillaries play a critical role in sensing neural activity and translating it into dynamic changes in cerebral blood flow to serve the metabolic needs of the brain. The molecular cornerstone of this mechanism is the capillary endothelial cell inward rectifier K$^+$ (Kir2.1) channel, which is activated by neuronal activity–dependent increases in external K$^+$ concentration, producing a propagating hyperpolarizing electrical signal that dilates upstream arterioles. Here, we identify a key regulator of this process, demonstrating that phosphatidylinositol 4,5-bisphosphate (PIP$_2$) is an intrinsic modulator of capillary Kir2.1-mediated signaling. We further show that PIP$_2$ depletion through activation of G$_q$ protein-coupled receptors (G$_q$PCRs) cripples capillary-to-arteriole signal transduction in vitro and in vivo, highlighting the potential regulatory linkage between G$_q$PCR-dependent and electrical neurovascular-coupling mechanisms. These results collectively show that PIP$_2$ sets the gain of capillary-initiated electrical signaling by modulating Kir2.1 channels. Endothelial PIP$_2$ levels would therefore shape the extent of retrograde signaling and modulate cerebral blood flow.

potassium channels | GPCR | cerebral blood flow | neurovascular coupling | PIP$_2$

Capillaries, the smallest of all blood vessels, are narrow (~5-μm diameter) tubes consisting of a single layer of endothelial cells arranged end to end. An examination of the mammalian brain angioarchitecture reveals a dense network of capillaries forming interconnected loops that lie in close apposition to all neurons (1, 2). This anatomical arrangement ideally positions capillaries to detect neuronal activity and communicate it to upstream arterioles. Notable in this context, we recently reported that increases in extracellular K$^+$ concentration ([K$^+$]$_o$), such as those evoked by neuronal activity, trigger an ascending hyperpolarizing signal that dilates upstream arterioles and enhances capillary red blood cell (RBC) flux and cerebral blood flow (3). The rapid transmission of signals from capillaries to arterioles serves to link local blood flow to the metabolic demands of active neurons; this process, termed neurovascular coupling, underlies use-dependent increases in local perfusion (functional hyperemia).

Our recent investigations of brain capillary endothelial cells (cECs) have revealed that the molecular basis for this capillary-to-arteriole signaling is the inward rectifier K$^+$ channel, Kir2.1, characterized by its activation by external K$^+$ and hyperpolarization (4). Because of these biophysical properties, Kir2.1 channels confer on capillary endothelial cells the ability to support neurovascular coupling by sensing increases in local [K$^+$]$_o$ to cause membrane potential hyperpolarization, which is transmitted through gap junctions to hyperpolarize adjacent endothelial cells. This hyperpolarizing signal is regenerated by virtue of the voltage dependence of Kir2.1 channels and propagates rapidly upstream to cause vasodilation (3). As critical as speed and regeneration are for the ability of retrograde vasodilatory signals to support functional hyperemia, they are only part of the story; a mechanism that determines the extent and directionality of the signal is also needed. Importantly, whether this electrical capillary-to-arteriole signal transduction mechanism intersects with other physiological stimuli implicated in neurovascular coupling—and, if so, how—is not known.

Among the various factors in addition to K$^+$ ions proposed to mediate neurovascular coupling are a number of agonists, including prostaglandin E$_2$ (PGE$_2$) (5, 6) and ATP (7, 8), that are capable of activating G protein-coupled receptors that signal through the Gα$_{q/11}$ subtype (G$_q$PCRs). Prototypically, activation of G$_q$PCRs stimulates phospholipase C (PLC), which hydrolyzes phosphatidylinositol 4,5-bisphosphate (PIP$_2$) to inositol 1,4,5-trisphosphate (IP$_3$) and diacylglycerol. The second messengers, IP$_3$ and diacylglycerol, are well-known to play major roles in intracellular signaling pathways through their activation of IP$_3$ receptors (IP$_3$Rs) and protein kinase C (PKC), respectively. However, the rapid and sustained decline in PIP$_2$ levels that accompanies PLC-mediated hydrolysis of PIP$_2$ is an often-overlooked consequence of G$_q$PCR activation, with important signaling implications (9–11).

The phosphoinositide PIP$_2$, a minor negatively charged phospholipid that resides primarily in the inner leaflet of the plasma membrane, is a well-established regulator of membrane proteins, including ion channels (11–15). In the case of Kir2 channels, crystallographic and structural studies have revealed that PIP$_2$ binds to specific positively charged residues of the channel, an association that is essential for channel activation (16–19). These observations suggest the possibility that alterations in PIP$_2$ levels by astrocyte- and/or neuron-derived G$_q$PCR agonists implicated in neurovascular coupling might modulate capillary electrical signaling. Despite the conceptual appeal of such a

Significance

Capillaries, the smallest blood vessels, mediate the on-demand delivery of oxygen and nutrients required to support the function of active cells throughout the brain. But how blood flow is directed to cells in active brain regions to satisfy their energy needs is poorly understood. We demonstrate that the plasma membrane phospholipid, PIP$_2$, is fundamental to sustaining the activity of inwardly rectifying potassium channels—the molecular feature that allows capillary endothelial cells to sense ongoing neuronal activity and trigger an increase in local blood flow. We further show that chemical factors released in the brain, including those associated with neuronal activity, cause changes in the levels of PIP$_2$, thereby altering endothelial potassium channel signaling and controlling cerebral blood flow.

PHYSIOLOGY

PIP$_2$–Kir2.1 relationship, whether it represents an intrinsic mechanism for regulating the activity of capillary endothelial cell Kir2.1 channels is not known.

Here, we demonstrate that PIP$_2$ is required for sustaining Kir2.1 activity in capillary endothelial cells. We further show that PIP$_2$ degradation, mediated by G$_q$PCR agonists implicated in neurovascular coupling, deactivates electrical capillary-to-arteriole signaling and alters cerebral blood flow. Collectively, our findings establish that perturbations in PIP$_2$ levels produced by physiologically relevant stimuli influence cerebral blood flow by determining the extent of capillary electrical signaling, a regulatory paradigm with potentially profound significance for neurovascular coupling control.

Results

Kir2.1 Channel Activity in Capillary Endothelial Cells Is Sustained by an ATP-Dependent Mechanism. Recent work in our laboratory demonstrated that Kir2.1 channels in capillary endothelial cells transduce electrical (hyperpolarizing) signals that rapidly dilate upstream arterioles and increase RBC flux, effects that are abrogated by selective knockdown of endothelial Kir2.1 channels (3). Here, we sought to investigate intracellular regulatory features of this Kir2.1 channel-dependent signaling mechanism. Kir2.1 currents were measured in freshly isolated C57BL/6J mouse brain capillary endothelial cells bathed in a 60-mM [K$^+$]$_o$ solution, used to increase Kir2.1 current amplitude. Under these conditions, the K$^+$ equilibrium potential (E$_K$) was −23 mV. Ionic currents were recorded in the voltage-clamp mode of the patch-clamp technique. A 300-ms voltage-ramp protocol (−140 to +40 mV from a holding potential of −50 mV) was applied, and currents were recorded using the conventional whole-cell configuration. Inward K$^+$ currents were detected at potentials negative to E$_K$ with little outward current positive to E$_K$, a characteristic

feature of Kir2.1 channels (Fig. 1A). Intriguingly, Kir2.1 currents gradually declined after electrical access to the cell interior was attained. Because the conventional whole-cell configuration allows exchange of intracellular contents with the patch pipette solution, this observation suggested that a factor necessary for the maintenance of Kir2.1 channel activity was dialyzed out of the cell. In support of this interpretation, Kir2.1 currents were sustained in experiments performed using the perforated-patch configuration, in which the cytoplasm remains intact (Fig. 1A). Under both conditions, these currents were abolished by the Kir channel blocker Ba^{2+} (100 μM) (Fig. S1), consistent with previous reports by us and others (3, 20–22).

The pipette solution used for initial whole-cell patch-clamp experiments lacked ATP, a fortuitous omission that led us to focus on a potential ATP-dependent mechanism in regulating Kir2.1 channel activity. Under these original conditions, Kir2.1 currents measured in cells dialyzed with a solution lacking Mg-ATP declined by ∼36% after 15 min compared with those recorded immediately after acquisition of whole-cell electrical access (time = t$_0$). In contrast, Kir2.1 currents recorded with 1 mM Mg-ATP included in the pipette (intracellular) solution showed no decrease over the same time frame (Fig. 1 A and B). The decline in Kir2.1 currents was sensitive to the intracellular concentration of ATP, such that lower levels of Mg-ATP (10 or 100 μM) in the patch pipette were insufficient to prevent it (Fig. 1C). In addition, Mg-ATP-γ-S (1 mM), a nonhydrolyzable analog of ATP, failed to avert current decay (Fig. 1C), implying that ATP hydrolysis is required to sustain Kir2.1 currents and suggesting the involvement of a kinase. However, pharmacological inhibitors of protein kinase C (PKC), G (PKG), or A (PKA) in the presence of 1 mM Mg-ATP (intracellular), which is substantially higher than the K$_{M, ATP}$ (Michaelis constant for ATP) for these protein kinases (23), had no significant effect on Kir2.1
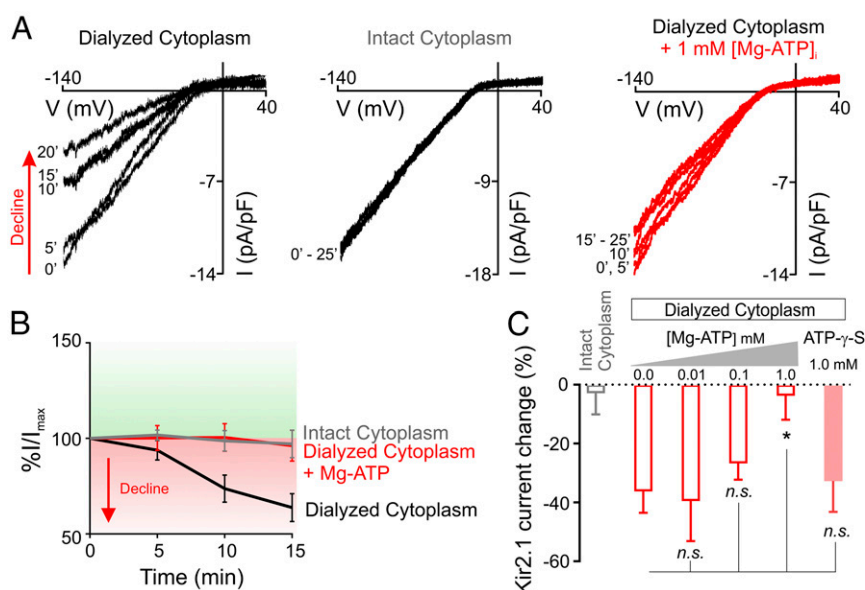

Fig. 1. Kir2.1 activity in capillary endothelial cells is sustained by an ATP-dependent mechanism. (A) Representative traces of Kir2.1 currents in freshly isolated capillary endothelial cells (cECs) bathed in 60 mM K$^+$, recorded from 0 to 20 or 25 min using voltage-ramps (−140 to 40 mV). (A, Left) Kir2.1 currents recorded in the conventional whole-cell configuration (dialyzed cytoplasm, 0 mM Mg-ATP in the pipette solution). (A, Middle) Kir2.1 currents recorded in the perforated whole-cell configuration (intact cytoplasm). (A, Right) Kir2.1 currents recorded in the conventional whole-cell configuration in a cEC dialyzed with 1 mM Mg-ATP. (B) Summary data showing normalized Kir2.1 currents over time, recorded at −140 mV in the conventional whole-cell configuration (dialyzed cytoplasm) with 0 mM Mg-ATP in the pipette solution (black line), in the perforated whole-cell configuration (intact cytoplasm; gray line), and in the conventional whole-cell configuration (dialyzed cytoplasm) with 1 mM Mg-ATP in the pipette solution (red line). Error bars represent SEM (n = 6–9 per condition). (C) Summary data showing the concentration dependence and hydrolysis requirement for Mg-ATP–mediated Kir2.1 current preservation (duration, 15 min). Values are presented as means ± SEM (*P < 0.05, one-way ANOVA followed by Dunnett's multiple comparisons test; n = 5–9 for Mg-ATP experiments and n = 4 for ATP-γ-S experiments). %I/I$_{max}$ is Kir2.1 current normalized to the maximum current (at t$_0$) and expressed as a percentage. n.s., not significant.

current decline (Fig. S2), arguing against a role for these protein kinases in sustaining capillary Kir2.1 activity.

Maintenance of PIP₂ Levels Through ATP-Dependent Phosphatidylinositol Kinase Activity Underlies Sustained Kir2.1 Channel Activity. Unlike protein kinases, most of which are maximally activated by low micromolar ATP concentrations, lipid kinases generally require much higher concentrations of ATP to support their activity (23–26). In light of the concentration dependence of intracellular ATP effects, noted above (Fig. 1C), and the well-known role of the phosphoinositide PIP_2 in regulating membrane proteins, including ion channels, we turned our attention to the phosphoinositide pathway. Endogenous PIP_2 levels are dynamically regulated by the opposing actions of lipid kinases and phosphatases (13, 24). The formation of PIP_2 reflects the sequential actions of phosphatidylinositol 4-kinase (PI4K), which converts phosphatidylinositol (PI) to phosphatidylinositol 4-phosphate (PIP), and phosphatidylinositol 4-phosphate 5-kinase (PIP5K), which converts PIP to PIP_2 (Fig. 2A). Phosphorylation of PI by PI4K is the rate-limiting step in PIP_2 synthesis, and Mg-ATP is required for the activity of PI4K ($K_{M, ATP} \approx 0.4$ to 1 mM) (25–27). To determine whether the decline in Kir2.1 channel activity observed in the absence of Mg-ATP could be traced back to depletion of PIP_2, we added the water-soluble, short-chain PIP_2 derivative, dioctanoyl-PIP_2 (hereafter, diC8-PIP_2), to the pipette solution in the conventional whole-cell configuration and measured Kir2.1 currents. Consistent with an essential role for PIP_2 in sustaining capillary Kir2.1 activity, inclusion of 10 µM diC8-PIP_2 largely abrogated the decline in Kir2.1 currents (Fig. 2 B and C). The initial current density (at t_0) was the same for the perforated-patch configuration and conventional whole-cell configuration dialyzed with or without Mg-ATP, or with diC8-PIP_2 and 0 mM Mg-ATP (Fig. 2D). The finding that diC8-PIP_2 did not elevate initial Kir2.1 currents suggests that these channels are saturated with PIP_2 under basal conditions.

Because replenishment of PIP_2 after depletion depends on PI4K and PIP5K activities and ATP hydrolysis (Fig. 2A), we next tested the effects of cell-permeable inhibitors of PIP_2 synthesis on Kir2.1 currents recorded in the perforated-patch (intact-cytoplasm) configuration. The PI4K inhibitors PIK93 (300 nM) and phenylarsine oxide (10 µM) significantly suppressed Kir2.1 currents under conditions in which intracellular ATP was unperturbed; inhibition of PIP5K with UNC3230 (100 nM) yielded similar results (Fig. 2 E and F). These findings collectively indicate that ATP-dependent synthesis of PIP_2 is essential for sustained Kir2.1 activity in brain capillaries.

GqPCR Stimulation Reduces Kir2.1 Currents by Decreasing PIP₂ Levels. PIP_2 is key to the maintenance of functional inward-rectifier K^+ channels, as indicated above (Figs. 1 and 2) and reported previously (12, 16, 17). Although PIP_2 is a minor phospholipid, it is nonetheless dynamic. Under physiological conditions, the primary driver of changes in PIP_2 levels is G_qPCR-mediated activation of PLC and subsequent hydrolysis of PIP_2 to IP_3 and diacylglycerol (Fig. 3A). A number of putative astrocyte-derived vasoactive substances implicated in neurovascular coupling, including PGE_2 and ATP (5–8), are G_qPCR agonists; thus, their signaling is capable of promoting PLC-mediated PIP_2 degradation. To determine whether activation of endothelial G_qPCRs suppresses Kir2.1 channels via PIP_2 hydrolysis, we examined Kir2.1 currents in dialyzed capillary endothelial cells (no ATP in the patch pipette) following treatment with PGE_2, which can signal through the prostanoid G_qPCR, EP_1 (28, 29). As shown in Fig. 3 B and C, application of PGE_2 (2 µM) to dialyzed cells accelerated the decay of Kir2.1 currents, almost doubling the extent of current decline after 15 min (62%), compared with that observed in matching time controls (36%) (Fig. 1C). Hindering PIP_2 synthesis through removal of Mg-ATP and enhancing its
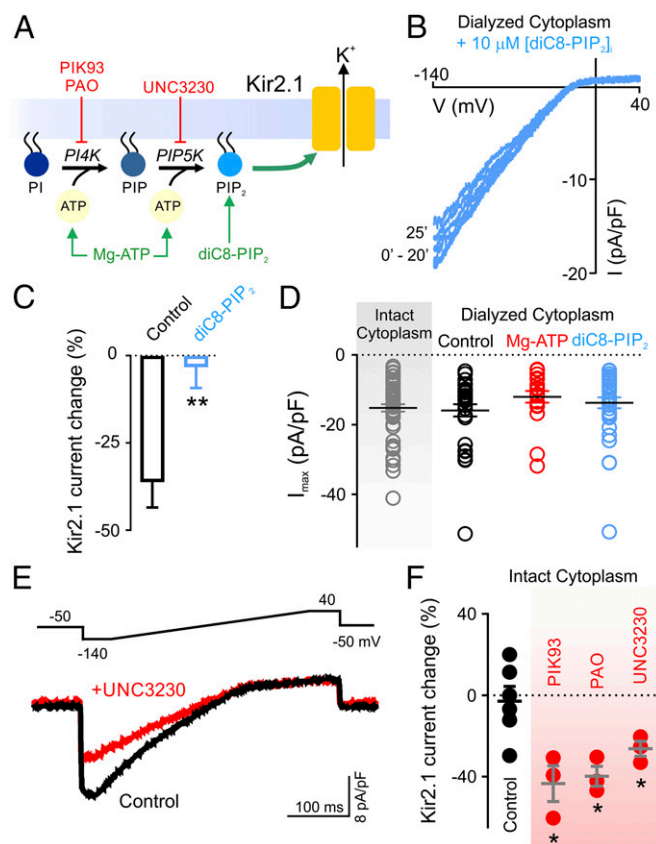

Fig. 2. Intracellular ATP and PIP_2 maintain Kir2.1 currents. (A) Schematic diagram showing the ATP-dependent synthesis steps and pharmacological interventions in the pathway leading to the production of PIP_2. (B) Representative traces of Kir2.1 currents recorded over 25 min in the conventional whole-cell configuration in a capillary endothelial cell (cEC) dialyzed with a pipette solution containing 0 mM Mg-ATP, with 10 µM diC8-PIP_2. (C) Changes in Kir2.1 currents over time, recorded in the conventional whole-cell configuration in cECs dialyzed with a pipette solution containing 0 mM Mg-ATP, with or without (control) 10 µM diC8-PIP_2. Currents obtained at 15 min are expressed as a percentage relative to those at t_0 (time of acquisition of whole-cell electrical access). Data are presented as means ± SEM (**$P < 0.01$ unpaired Student's t test, $n = 9$–10). (D) Individual-value plots of peak inward currents in cECs, measured at −140 mV (at t_0) using the perforated whole-cell configuration (intact cytoplasm; gray) or conventional whole-cell configuration in cECs dialyzed with a pipette solution containing 0 mM Mg-ATP (black), 1 mM Mg-ATP (red), or 0 mM Mg-ATP + 10 µM diC8-PIP_2 (blue). Whole-cell capacitance averaged 8.6 pF. There were no significant differences among groups (one-way ANOVA followed by Dunnett's multiple comparisons test, $n = 19$–57). (E) Representative traces of Kir2.1 currents in a cEC with intact cytoplasm (perforated configuration) before (control) and 15 min after incubation with the PIP5K inhibitor UNC3230 (100 nM). (F) Individual-value plots showing effects of the PIP_2 synthesis inhibitors PIK93 (PI4K inhibitor, 300 nM), PAO (PI4K inhibitor, 10 µM), and UNC3230 (PIP5K inhibitor, 100 nM) on Kir2.1 currents in cytoplasm-intact cECs. Inhibitors were bath-applied immediately after t_0, and currents were compared before and 15 min after incubation (*$P < 0.05$, one-way ANOVA followed by Dunnett's multiple comparisons test).

breakdown through activation of a G_qPCR should decrease ambient PIP_2 levels and thus inhibit Kir2.1 channel activity. Accordingly, to calculate the time constant of Kir2.1 current decay (τ_{decay}), we monitored Kir2.1 currents over time following application of a PIP_2-depleting G_qPCR agonist onto capillary endothelial cells dialyzed with 0 mM Mg-ATP. Using this experimental approach, we estimated a τ_{decay} of ~7 to 13 min, which reflects the change in PIP_2 synthesis and breakdown. Note that, under these conditions, Kir2.1 current was not completely
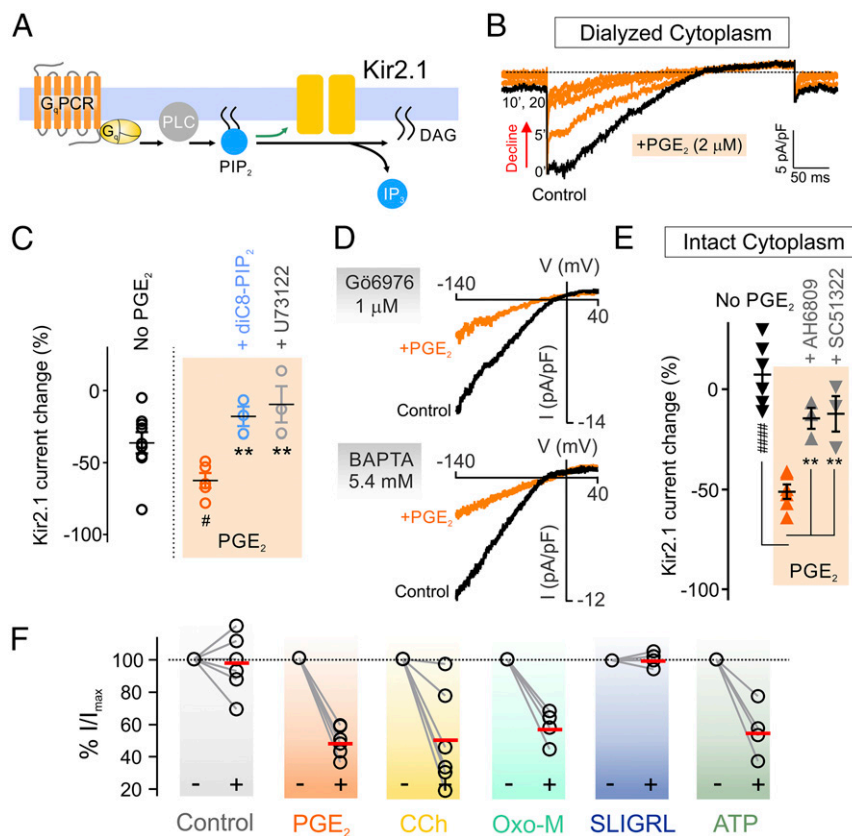
PHYSIOLOGY

Fig. 3. PGE$_2$ inhibits Kir2.1 current in cECs by reducing PIP$_2$ levels. (*A*) Schematic depiction of PIP$_2$ depletion by G$_q$PCR activation through PLC-mediated hydrolysis to IP$_3$ and diacylglycerol (DAG). (*B*) Representative traces of Kir2.1 currents in a dialyzed capillary endothelial cell (cEC; 0 mM Mg-ATP) at different time points after addition of PGE$_2$ (2 μM) showing accelerated current decline following G$_q$PCR activation. (*C*) Individual-value plots showing the enhancement of cEC Kir2.1 current decline by bath-applied PGE$_2$ (2 μM; $n = 5$) compared with time controls (no PGE$_2$; $n = 9$; [#]$P < 0.05$ unpaired Student's t test) and rescue by 10 μM diC8-PIP$_2$ (dialyzed; $n = 3$) or 10 μM U73122 (bath-applied; $n = 3$). Currents were recorded upon access to the cell interior (t_0) and after 15 min in cECs dialyzed with 0 mM Mg-ATP-pipette solution. Changes in Kir2.1 currents were calculated as values obtained at 15 min relative to those at t_0, expressed as a percentage. Individual data points are shown together with means (long horizontal lines) and SEM (error bars) (**$P < 0.01$, one-way ANOVA followed by Dunnett's multiple comparisons test). (*D*) Representative current traces showing no effect of the PKC inhibitor Gö6976 (1 μM; bath-applied) or rapid cytosolic Ca^{2+} chelation with BAPTA (5.4 mM; dialyzed) on the PGE$_2$-induced decline of Kir2.1 currents in cECs dialyzed with 0 mM Mg-ATP. (*E*) Individual-value plots showing the effects of the prostanoid receptor blockers AH6809 (10 μM, $n = 3$) and SC51322 (1 μM, $n = 3$) on the enhancement of Kir2.1 current decline in cECs by PGE$_2$, recorded under cytoplasm-intact conditions over a 15-min period. Changes in Kir2.1 currents were calculated as values obtained at 15 min relative to those at t_0, expressed as a percentage. Individual data points are shown together with means (long horizontal lines) and SEM (error bars) ([####]$P < 0.0001$, unpaired Student's t test, $n = 6$; **$P < 0.01$, one-way ANOVA followed by Dunnett's multiple comparisons test). (*F*) Effects of G$_q$PCR agonists on normalized Kir2.1 current decline in cECs. Kir2.1 currents were recorded in the perforated patch configuration over 15 min in the absence (control) or presence of bath-applied PGE$_2$ (2 μM), carbachol (CCh, 10 μM), oxotremorine M (Oxo-M, 10 μM), SLIGRL-NH$_2$ (5 μM), or ATP (30 μM). Red horizontal lines indicate means ($n = 4$–6 each).

abolished (∼60 to 70% inhibition), suggesting residual ongoing PIP$_2$ synthesis. These slow decay kinetics (spanning minutes) are consistent with the high affinity of PIP$_2$ for Kir2.1 channels (18, 19, 30, 31).

Introduction of diC8-PIP$_2$ (10 μM) into the cytosol or inhibition of PLC with U73122 (10 μM) are interventions that serve to compensate for or prevent PLC-dependent PIP$_2$ degradation, respectively. Both maneuvers completely abrogated the PGE$_2$-induced reduction in Kir2.1 current (Fig. 3*C*), confirming the involvement of PIP$_2$ hydrolysis downstream of activation of the G$_q$PCR-PLC pathway in the decay of Kir2.1 activity. The effect of PIP$_2$ hydrolysis on Kir2.1 channel activity was not attributable to the engagement of signaling pathways mediated by the PIP$_2$ breakdown products IP$_3$ or diacylglycerol. Neither rapid chelation of cytoplasmic Ca^{2+} with intracellular 1,2-bis(2-aminophenoxy)ethane-*N*,*N*,*N*′,*N*′-tetraacetic acid (BAPTA) (5.4 mM) nor inhibition of protein kinase C with 12-(2-cyanoethyl)-6,7,12,13-tetrahydro-13-methyl-5-oxo-5H-indolo(2,3-a)pyrrolo(3,4-c)-carbazole (Gö6976) (1 μM) attenuated the PGE$_2$-mediated

suppression of Kir2.1 currents (Fig. 3*D*). Along the same lines, simultaneous blockade of both diacylglycerol-PKC and IP$_3$-IP$_3$R-Ca^{2+} signaling cascades failed to impact the inhibitory effect of PGE$_2$ on Kir2.1 current in dialyzed capillary endothelial cells (Fig. S3). Taken together, these data show that PGE$_2$ acts through G$_q$PCR activation to stimulate PLC and decrease PIP$_2$ levels, thereby deactivating Kir2.1 channels independently of PIP$_2$ metabolites.

An important confirmation of this conclusion was provided by experiments performed in cytoplasm-intact mode (perforated patch), in which endogenous ATP and PIP$_2$ are not perturbed and Kir2.1 currents were found to be resistant to decline (Figs. 1*A* and 3*E*). These experiments showed that application of the G$_q$PCR agonist PGE$_2$ rapidly (onset, <60 s) and dramatically reduced Kir2.1 currents (∼51% decline) (Fig. 3*E*), consistent with the idea that G$_q$PCR stimulation exerts an inhibitory effect on Kir2.1 channel activity. The inhibitory effect of PGE$_2$ was prevented by the nonselective prostanoid receptor (EP$_1$/EP$_2$/EP$_3$) antagonist AH6809 (10 μM) and, notably, by the selective

EP$_1$ antagonist SC51322 (1 µM), suggesting that PGE$_2$ acts through the G$_q$–coupled EP$_1$ receptor to inhibit capillary Kir2.1 channel activity (Fig. 3E).

To assess the generalizability of this mechanism, we compared changes in Kir2.1 currents induced by PGE$_2$ with those induced by muscarinic receptor agonists, the protease-activated receptor-2 (PAR2) agonist SLIGRL-NH$_2$, and the purinergic receptor agonist ATP, all of which are capable of signaling through G$_q$PCRs. Using capillary endothelial cells in the cytoplasm-intact mode (perforated patch), we found that the muscarinic receptor agonists carbachol and N,N,N-trimethyl-4-(2-oxo-1-pyrolidinyl)-2-butyn-1-ammonium iodide (oxotremorine M) (10 µM each) and purinergic receptor agonist ATP (30 µM) decreased Kir2.1 currents by 48 ± 12%, 40 ± 5%, and 43 ± 8%, respectively, after a 15-min incubation. These effects were comparable with those induced by PGE$_2$ (51 ± 4%) under similar experimental conditions (Fig. 3F). Interestingly, although SLIGRL-NH$_2$ has been shown to cause endothelial-dependent dilation of surface cerebral arteries (32), this PAR2 agonist (5 µM) had no effect on capillary Kir2.1 currents (Fig. 3F), possibly reflecting rapid receptor desensitization and a rebound in PIP$_2$ levels following activation (33). It is also possible that differences in receptor expression levels, requirements for specific localization patterns, and/or differential G$_q$PCR-dependent mobilization of PIP$_2$ contributes to G$_q$PCR agonist efficacy (9, 34, 35).

G$_q$PCR Stimulation Suppresses Capillary-to-Arteriole Electrical Signaling.

Capillary Kir2.1 channels sense increases in [K$^+$]$_o$ caused by increased neuronal activity and initiate a hyperpolarizing signal. By virtue of strong electrical coupling between endothelial cells, retrograde hyperpolarization ascends to upstream feeding arterioles to enhance cerebral blood flow to the site of signal initiation (3). The fact that G$_q$PCR activation suppresses Kir2.1 currents in capillary endothelial cells (Fig. 3) suggests that G$_q$PCR agonists could alter capillary-to-arteriole signaling and ensuing changes in blood flow. To investigate this possibility, we used our recently developed ex vivo capillary-parenchymal arteriole (CaPA) preparation, which makes it possible to monitor effects of local stimulation of capillary branches on upstream arteriolar diameter in a reduced environment (3). Focal stimulation of capillaries in the CaPA preparation with 10 mM K$^+$ induced a reproducible dilatory response in the attached arteriolar segment (Fig. 4A), reflecting activation of capillary Kir2.1 channels (3). To test the influence of G$_q$PCR signaling on Kir2.1-mediated capillary-to-arteriole signaling, we bath-applied the postulated neurovascular coupling agent PGE$_2$ (1 µM) to globally activate EP$_1$ receptors and degrade PIP$_2$. Consistent with PIP$_2$ breakdown and disabling of Kir2.1 channels, PGE$_2$ gradually attenuated and, ultimately, abolished K$^+$-induced upstream vasodilation (Fig. 4A). Capillary Kir2.1-mediated upstream arteriolar dilation was similarly suppressed by the muscarinic receptor agonist carbachol (Fig. S4). Capillary responsiveness to elevated external K$^+$ recovered after removal of PGE$_2$ from the capillary-parenchymal arteriole preparation ($\tau_{recovery} \approx 17$ min) (Fig. 4A). The latter observation is consistent with the idea that the PIP$_2$ necessary for Kir2.1 channel activity was replenished during the period between PGE$_2$ washout and subsequent remeasurement. Notably, there was a lag phase (X$_0 \approx$ 18 min) between PGE$_2$ application and onset of the inhibition of capillary-mediated arteriolar dilation (Fig. 4B). During this lag period, Kir2.1 currents recorded in the perforated-patch configuration declined steadily ($\tau_{decay} \approx 12$ min), but K$^+$-mediated retrograde dilatory signaling remained intact until Kir2.1 currents
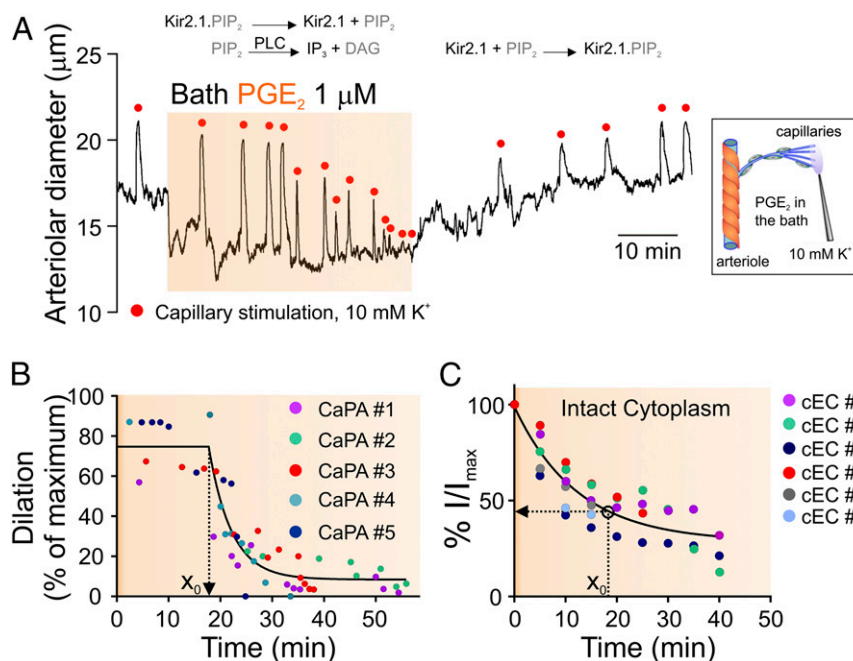
Fig. 4. G$_q$PCR stimulation cripples capillary-to-arteriole electrical signaling. (A) Representative diameter recording showing the time course of the inhibitory effect of bath-applied PGE$_2$ (1 µM) on upstream arteriolar dilations induced by successive focal applications of 10 mM K$^+$ (18 s, 5 psi) onto capillary segments in a capillary-parenchymal arteriole (CaPA) preparation (schematic, Right Inset). Relations above the trace indicate the processes occurring in the presence of PGE$_2$ [dissociation of PIP$_2$ from Kir2.1 and hydrolysis of PIP$_2$ to diacylglycerol (DAG)] and washout (reassociation of PIP$_2$ with Kir2.1). (B) Summary data for experiment in A, showing K$^+$-induced dilations from five CaPA preparations (n = 5 mice), calculated as a percentage of maximal diameter responses (obtained in 0 mM Ca^{2+} at the conclusion of each experiment). Results were best fit as a plateau (lag phase) followed by one-phase exponential decay ($R^2 = 0.85$). Lag phase (X$_0$) ≈ 18 min; time constant of the postplateau exponential decay phase (τ_{decay}) ≈ 4 min. (C) Kir2.1 current decline following application of 2 µM PGE$_2$ onto capillary endothelial cells (cECs) at t_0 (i.e., upon achieving electrical access), recorded in the perforated-patch (intact cytoplasm) configuration. Time constant of the exponential decay phase (τ_{decay}) ≈ 12 min (one-phase exponential decay, $R^2 = 0.85$). Note the absence of a lag phase for Kir2.1 current decline. At X$_0$ (18 min), corresponding to the lag phase before detecting a decrease in dilatory response (in B), Kir2.1 current had declined by ~53%.

reached ∼50% of their maximal amplitude (Fig. 4C). These observations suggest that a critical number of Kir2.1 channels must deactivate to impact the regenerative propagation of hyperpolarization from capillaries to the upstream arteriole.

In Vivo G_qPCR Stimulation Inhibits K^+-Evoked Capillary Hyperemia.
Raising $[K^+]_o$ around capillaries in vivo evokes upstream arteriolar dilation and increases capillary RBC flux (3). Stimulation of G_qPCRs inhibits Kir2.1 channels and capillary-to-arteriole signaling in the ex vivo capillary-parenchymal arteriole preparation (Figs. 3 and 4 and Fig. S4). Building on these results, we sought to determine whether activation of endothelial cell G_qPCRs by systemic administration of a suitable agonist alters responses to elevated $[K^+]_o$ in vivo, measured by imaging RBC flux in mice using a cranial window model. For these experiments, we chose to use carbachol, which exerted inhibitory effects on capillary Kir2.1 currents (Fig. 3 and Fig. S4) and Kir2.1-mediated capillary-to-arteriole signaling (Fig. S4) similar to those evoked by PGE_2. The rationale for using carbachol over PGE_2 during in vivo imaging is multifold. First, carbachol is a positively charged choline carbamate with a characteristically lipophobic structure. Carbachol is thus unable to cross the blood–brain barrier (BBB), a property that is key to our experimental goal of influencing brain endothelial cells without directly affecting other brain cells. In contrast, prostaglandins are highly lipophilic; PGE_2, in particular, crosses the BBB (36) and can contribute to pathological BBB breakdown (37). Second, PGE_2, which can be synthesized in the brain endothelium (38), is highly pyrogenic and exerts proinflammatory actions through multiple effects on different cell types (39, 40). Third, PGE_2 evokes mixed vasomotor effects that may interfere with our question of interest: for example, constricting isolated brain parenchymal arterioles, as we have previously reported (29), but dilating other vascular beds, as reported by others (6, 41, 42). Such mixed vasomotor effects can lead to alterations in blood pressure and could thus introduce a confounding factor to in vivo experiments. Carbachol, in contrast, minimally altered parenchymal arteriolar diameter (Fig. S4), and, at the lower systemic dosage employed here, has no effect on arterial blood pressure or partial pressures of O_2 or CO_2 in the blood (43).

Anesthetized mice were fitted with a cranial window and systemically injected with fluorescein isothiocyanate (FITC)-labeled dextran to allow visualization of the vascular network and support contrast imaging of RBCs by two-photon laser-scanning microscopy (Fig. 5A). Mice were divided into two experimental groups: saline-treated (time-control) and carbachol-treated. Mice in the carbachol-treated group were systemically administered a low dose (0.6 μg/kg body weight) of carbachol via intravascular injection into the retroorbital venous sinus to activate endothelial muscarinic G_qPCRs. Mice in the control group were similarly administered saline. K^+-evoked, Kir2.1-mediated hyperemia was investigated in both groups before (baseline) and 10, 20, and 30 min after injection. Focal stimulation of a brain capillary in control mice by pressure ejection (300 ms) of 10 mM K^+ via a micropipette evoked a rapid increase ($52 \pm 12\%$ at t = 20 min post-saline administration) in capillary RBC flux in the stimulated segment (Fig. 5 B and C). As predicted based on ex vivo results, circulating carbachol profoundly decreased the in vivo response to 10 mM K^+, yielding a K^+-induced increase in RBC flux ($10 \pm 6\%$ at t = 20 min after carbachol injection) more than fivefold lower than that in controls (Fig. 5 B–E). Baseline capillary RBC flux (before K^+ application) did not change in the carbachol-injected group over the course of 30 min (Fig. S5A). The diameters of parenchymal arterioles upstream of the tested capillary segments were not changed by a 20-min carbachol treatment compared with that in the saline (time-control) group (Fig. S5B). At the conclusion of each 30-min experiment, application of a 0-mM Ca^{2+} solution containing 200 μM diltiazem

(included to inhibit arterial/arteriolar Ca^{2+} channels) to the cranial surface dramatically dilated arterioles and enhanced capillary RBC flux in both saline- and carbachol-treated groups (Fig. 5C and Fig. S5). This latter observation is important because it indicates that vasodilatory and RBC flux response are not already maximal, confirming that the lack of a hyperemic response to external K^+ postcarbachol treatment is attributable to Kir2.1 channel deactivation.

Discussion

Capillary endothelial cells in the brain are anatomically positioned to sense neuronal activity and orchestrate the matching of cerebral blood flow to the moment-to-moment metabolic demands of the brain. They are also equipped with the molecular machinery—Kir2.1 channels and G_qPCRs—necessary to respond to factors—K^+ and G_qPCR agonists—that have been implicated in neurovascular coupling. We recently reported that Kir2.1 channels in brain capillary endothelial cells function as K^+ sensors. Increases in $[K^+]_o$ associated with neuronal activity trigger an ascending hyperpolarizing signal that dilates upstream arterioles and enhances capillary RBC flux and cerebral blood flow (3). The present study sheds light on the molecular features that regulate this electrical signaling. Specifically, our results show that PIP_2 levels are critical determinants in sustaining Kir2.1 channel activity in the brain capillary endothelium, supporting the concept that this phosphoinositide plays a central role in regulating Kir2.1 channel-mediated electrical signaling during neurovascular coupling. We extend this concept and provide strong evidence for the existence of communication from G_qPCRs to this electrical signaling mechanism, reflecting the dependence of Kir2.1 channel structure and function on cellular PIP_2 and the ability of G_qPCRs to deplete it. Importantly, we further show that G_qPCR stimulation short-circuits the ascending electrical signal originating at the capillary level and abrogates upstream dilation, both ex vivo (Fig. 4) and in vivo (Fig. 5). This paradigm establishes PIP_2 as a point of intersection between G_qPCR-mediated signaling and electrical signaling. This model uniquely highlights the role of G_qPCRs as a signaling "switch" with the potential to determine the extent and directionality of the electrical signaling modality in brain capillaries and ultimately modulate functional hyperemic responses.

PIP_2 has been shown to bind to and modulate a plethora of ion channels, including members of the Kir2 channel family (13). An important feature of PIP_2 is that its cellular levels are dynamically regulated through continuous synthesis by lipid kinases and breakdown by lipases. PIP_2 is synthesized by the lipid kinases PI4K and PIP5K, which convert PI to PIP and PIP to PIP_2, respectively. This process is highly ATP concentration-dependent, reflecting the relatively low ATP affinity of these lipid kinases (23, 25, 26). Consistent with this, our results indicate that sustaining the PIP_2 levels necessary to support Kir2.1 channel activity is critically dependent on the intracellular concentration of ATP. On the breakdown side of this equation, PLC, activated in response to stimulation of G_qPCRs, hydrolyzes PIP_2 to IP_3 and diacylglycerol. It has been shown that G_qPCR-mediated depletion of PIP_2 is capable of altering the activity of PIP_2-regulated channels (44), suggesting that persistent depletion of this minor (∼1%) plasma membrane phospholipid in capillary endothelial cells would have major consequences for Kir2.1 activity. Indeed, we found that multiple G_qPCR agonists, including those implicated in neurovascular coupling (PGE_2 and ATP) (5–8), are capable of deactivating Kir2.1 currents (Fig. 3). Our data also confirmed that the ability of G_qPCR agonists to suppress capillary Kir2.1 channel activity in the capillary endothelium is not attributable to IP_3-IP_3R-Ca^{2+} or diacylglycerol-PKC signaling (Fig. 3 and Fig. S3). Notably, enhanced G_qPCR/PLC activation can promote PIP_2 breakdown at rates that exceed ongoing synthesis (Fig. 3 E and F). The differential kinetics of PIP_2 hydrolysis
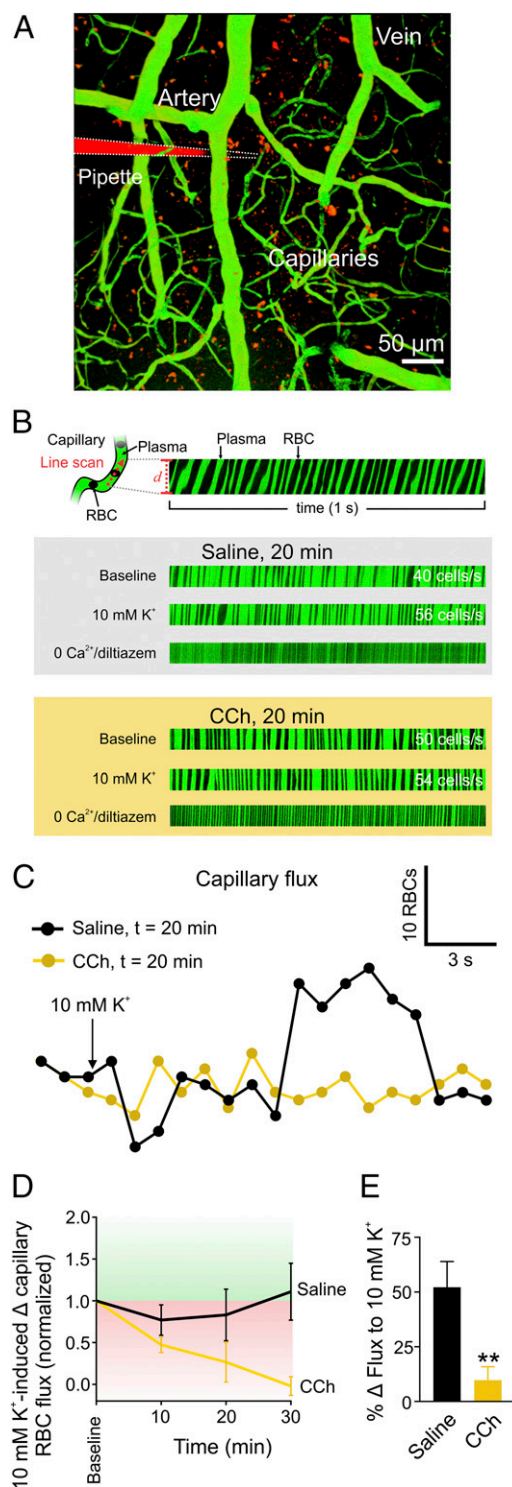
Fig. 5. Activation of cEC muscarinic receptors attenuates K$^+$-induced increases in capillary RBC flux in vivo. (*A*) A 3D projection depicting the positioning of a pipette containing artificial cerebrospinal fluid with 10 mM K$^+$ and TRITC-dextran (red) adjacent to a brain cortex capillary in vivo. Green, FITC-dextran circulating in blood plasma. (*B*, *Top*) Raw capillary line-scan data showing RBCs (black streaks) in plasma (green); the *x* axis is time and the *y* axis is scanned capillary distance (*d*). (*B*, *Middle* and *Bottom*) Line scans at baseline and in response to ejection of K$^+$ (10 mM) onto the target capillary in a control (saline-injected) mouse and a mouse injected with carbachol (CCh, 0.6 μg/kg). Mice were systemically administered saline or CCh 20 min before applying 10 mM K$^+$ by pressure ejection. At the conclusion of experiments, 0 mM Ca^{2+}/200 μM diltiazem was applied to the brain surface

and repletion align with previous direct in vitro measurements, as well as in silico calculations (9), and are important when considering the long-lasting effects of endogenous G$_q$PCR agonists.

Our electrophysiological experiments illustrate that initial Kir2.1 channel activity was similar in dialyzed capillary endothelial cells, with or without PIP$_2$ supplementation (Fig. 2), implying that Kir2.1 channels are saturated with PIP$_2$ under basal conditions. These findings are consistent with structural studies of Kir2 channels, including reports of the crystal structure of the Kir2.2 channel (17), which have collectively established that these channels require PIP$_2$ binding to maintain their active conformation (16). In keeping with the reported high PIP$_2$-Kir2.1 affinity and/or specificity (16, 30, 45), we found that the kinetics of capillary Kir2.1 channel deactivation following G$_q$PCR activation or lowering of intracellular ATP levels are slow, consistent with high affinity binding. Nonetheless, our data clearly indicate that sustained G$_q$PCR activation is capable of causing sufficient PIP$_2$ dissociation to deactivate Kir2.1 channels.

The slow kinetics of Kir2.1 channel inhibition and the corresponding requirement for sustained G$_q$PCR activation to deplete PIP$_2$ sufficiently to deactivate the channel raise questions about the circumstances under which capillaries would experience prolonged exposure to receptor agonist. Given that brain capillaries are positioned in close proximity to all neurons and astrocytes (1, 2), capillaries are presumably exposed to a microenvironment containing potential physiological stimuli, including varying concentrations of G$_q$PCR agonists postulated to serve as neurovascular coupling agents. Moreover, rates of receptor-mediated PIP$_2$ breakdown exceed those of PIP$_2$ resynthesis, indicating that such G$_q$PCR agonists could trigger an extended decline in PIP$_2$ levels (9). Viewed from this perspective, G$_q$PCR-mediated PIP$_2$ depletion represents a potential entry point for local microenvironmental influences to dampen capillary Kir2.1-mediated electrical signaling (Fig. S6). G$_q$PCR signaling is also associated with initiation of an intracellular Ca^{2+} signal, reflecting IP$_3$ generation and Ca^{2+} release from intracellular stores. This suggests that astrocyte- and/or neuron-derived agonists implicated in neurovascular coupling could also engage a Ca^{2+} signaling-based mechanism in capillary endothelial cells. It is thus conceivable that, in addition to setting the gain of electrical signaling in brain capillaries, activation of capillary G$_q$PCRs by putative neurovascular coupling agents might also initiate a Ca^{2+} signal that could play a role in functional hyperemia.

Intriguingly, experiments using the capillary-parenchymal arteriole preparation showed that G$_q$PCR activation inhibited capillary Kir2.1-mediated upstream arteriolar dilation only after a lag phase, during which Kir2.1 currents, measured in isolated endothelial cells, steadily declined. An electrophysiological analysis of endothelial cells using the intact-cytoplasm configuration showed that the duration of this lag phase corresponded to the time required for deactivation of ~50% of Kir2.1 channels. These observations suggest that there is a minimum Kir2.1 channel density below which retrograde electrical signaling cannot

to evoke near-maximal arteriolar dilation and increase blood flow to the capillary bed to provide a frame of reference for the modest and submaximal increases in basal RBC flux sometimes observed in CCh-injected mice. (*C*) Time course of capillary RBC flux corresponding to the experiments in *B* in response to ejection of K$^+$ (10 mM) onto a capillary in a control (saline-injected) and a CCh-treated mouse, showing elimination of K$^+$-induced dilation by activation of capillary endothelial cell muscarinic receptors. (*D*) Changes in K$^+$ (10 mM)-induced capillary RBC flux over 30 min in saline- and CCh-treated mice (*n* = 6–7). Changes in flux at 10, 20, and 30 min were normalized to their respective baseline values. (*E*) Summary data showing the percentage change in RBC flux in response to K$^+$ (10 mM) 20 min after saline (*n* = 5) or CCh (*n* = 7) treatment (**$P < 0.01$, unpaired Student's *t* test).

occur. There are two conceptual scenarios in which the existence of such a threshold in Kir2.1 channel number could come into play. First, the originating endothelial cells may not move toward the K^+ equilibrium potential (E_K) upon exposure to elevated $[K^+]_o$—a requirement for initiating propagating hyperpolarization—if outward current through Kir2.1 channels is below a critical level. Alternatively, distant capillary endothelial cells may be unable to support the regenerative propagation of hyperpolarization if Kir2.1 current falls below a certain point. Experimental and computational modeling investigations are required to determine which scenario more accurately describes G_qPCR-induced suppression of capillary electrical signaling.

One implication of the ATP concentration-dependent synthesis of PIP_2 is that modest decreases in ATP that would have no effect on high ATP affinity cellular reactions could compromise ongoing phosphoinositide repletion. In certain pathological settings, energy production is compromised, and cellular ATP levels in the brain decrease. Cerebral ischemia, for example, triggers a profound drop in $[ATP]_i$ (46, 47), which would be expected to suppress electrical signaling through Kir2.1 channels. Another example is cortical spreading depression, in which a slow wave of depolarization propagates across the cerebral cortex. This wave is associated with decreased glucose and ATP levels, along with global neurotransmitter release and, presumably, subsequent G_qPCR activation (48). These latter observations offer alternative avenues for PIP_2 depletion through changes in the brain metabolic status; whether this will affect capillary signaling awaits confirmation.

Collectively, the results presented here provide strong evidence for a novel paradigm in which PIP_2 is a central player in the regulation of capillary endothelial signaling. Maintaining sufficient PIP_2 levels ensures proper capillary-to-arteriole electrical signaling whereas physiological or pathological decreases in the levels of this phospholipid would determine the strength and extent of this signaling, thereby impacting cerebral blood flow.

Materials and Methods

Animals. Adult (2- to 3-mo-old) male C57BL/6J mice (The Jackson Laboratory) were group-housed on a 12-h light:dark cycle with environmental enrichment and free access to food and water. All animals were euthanized by i.p. injection of sodium pentobarbital (100 mg/kg), followed by rapid decapitation. All procedures received prior approval from the University of Vermont Institutional Animal Care and Use Committee.

Chemicals. 5-[(Cyclohexylcarbonyl)amino]-2-(phenylamino)-thiazolecarboxamide (UNC-3230), and N,N,N-trimethyl-4-(2-oxo-1-pyrolidinyl)-2-butyn-1-ammonium iodide (oxotremorine M) were obtained from Tocris Bioscience. 1,2-Dioctanoyl phosphatidylinositol 4,5-bisphosphate sodium salt (diC8-PIP$_2$) was purchased from Cayman Chemical, and 12-(2-cyanoethyl)-6,7,12,13-tetrahydro-13-methyl-5-oxo-5H-indolo(2,3-a)pyrrolo(3,4-c)-carbazole (Gö6976) was from Calbiochem. Unless otherwise noted, all other chemicals were obtained from Sigma-Aldrich.

Capillary Endothelial Cell Isolation. Single capillary endothelial cells (cECs) were obtained from mouse brains by mechanical disruption of two 160-μm-thick brain slices using a Dounce homogenizer, as previously described (3). Slices were homogenized in ice-cold artificial cerebrospinal fluid, with the composition 124 mM NaCl, 3 mM KCl, 2 mM CaCl$_2$, 2 mM MgCl$_2$, 1.25 mM NaH$_2$PO$_4$, 26 mM NaHCO$_3$, and 4 mM glucose. Debris was removed by passing the homogenate through a 62-μm nylon mesh. Retained capillary fragments were washed into dissociation solution, composed of 55 mM NaCl, 80 mM Na-glutamate, 5.6 mM KCl, 2 mM MgCl$_2$, 4 mM glucose, and 10 mM Hepes (pH 7.3) containing neutral protease (0.5 mg/mL), elastase (0.5 mg/mL; Worthington), and 100 μM CaCl$_2$, and incubated for 24 min at 37 °C. Following this step, 0.5 mg/mL collagenase type I (Worthington) was added, and the solution was incubated for an additional 2 min at 37 °C. The suspension was filtered and washed to remove enzymes, and single cells and small capillary fragments were dispersed by triturating four to seven times with a fire-polished glass Pasteur pipette. Cells were used within ~6 h after dispersion.

Electrophysiology. Whole-cell currents were recorded using a patch-clamp amplifier (Axopatch 200B; Molecular Devices), filtered at 1 kHz, digitized at 5 kHz, and stored on a computer for offline analysis with Clampfit 10.3 software. Whole-cell capacitance was measured using the cancellation circuitry in the voltage-clamp amplifier. Electrophysiological analyses were performed in either the conventional or perforated whole-cell configuration. Recording pipettes were fabricated by pulling borosilicate glass (1.5-mm outer diameter, 1.17-mm inner diameter; Sutter Instruments) using a Narishige puller. Pipettes were fire-polished to a tip resistance of ~4 to 6 MΩ. The bath solution consisted of 80 mM NaCl, 60 mM KCl, 1 mM MgCl$_2$, 10 mM Hepes, 4 mM glucose, and 2 mM CaCl$_2$ (pH 7.4). For the conventional whole-cell configuration, pipettes were backfilled with a solution consisting of 10 mM NaOH, 11.4 mM KOH, 128.6 mM KCl, 1.1 mM MgCl$_2$, 2.2 mM CaCl$_2$, 5 mM EGTA, and 10 mM Hepes (pH 7.2). As noted in *Results*, the pipette solution was supplemented in some experiments with ATP (10 μM, 100 μM, or 1 mM) or ATP-γ-S (1 mM). In a subset of experiments (Fig. S7), Na-GTP (100 μM) was added to the pipette solution alone or together with 1 mM Mg-ATP; in neither setting did Na-GTP have an effect on peak Kir2.1 current amplitude or the kinetics of current decline. In a subset of experiments, BAPTA (5.4 mM) was used in place of EGTA. For perforated-patch electrophysiology, the pipette solution was composed of 10 mM NaCl, 26.6 mM KCl, 110 mM K^+ aspartate, 1 mM MgCl$_2$, 10 mM Hepes, and 200 to 250 μg/mL amphotericin B, added freshly on the day of the experiment.

Ex Vivo Capillary-Parenchymal Arteriole Preparation. The capillary-parenchymal arteriole (CaPA) preparation was obtained by dissecting parenchymal arterioles arising from the M1 region of the middle cerebral artery, leaving the attached capillary bed intact, as we reported recently (3). Precapillary arteriolar segments were cannulated on glass micropipettes on a Living Systems Instrumentation pressure myograph, with one end occluded by a tie. The ends of the capillaries were then sealed by the downward pressure of an overlying glass micropipette. Application of pressure (40 mmHg) to the cannulated parenchymal arteriole segment in this preparation pressurized the entire tree and induced myogenic tone in the parenchymal arteriole segment. With this preparation, 10 mM K^+ was applied onto capillaries by pressure ejection from a glass micropipette (tip diameter, ~5 μm) attached to a Picospritzer III (Parker) at ~5 psi for 18 s. Luminal diameter in parenchymal arterioles was acquired in one region of the arteriolar segment at 15 Hz using IonWizard 6.2 edge-detection software (IonOptix). Changes in arteriolar diameter were calculated from the average luminal diameter measured over the last 10 s of stimulation and were normalized to the maximum dilatory responses in 0 mM Ca^{2+} bath solution at the end of each experiment.

In Vivo Cerebrovascular and Hemodynamics Imaging. Mice were anesthetized with isoflurane (5% induction, 2% maintenance), essentially as described previously (3). Upon obtaining surgical-plane anesthesia, the skull was exposed, and a stainless-steel head plate was attached over the left hemisphere using dental cement. The head plate was secured in a holding frame, and a small (~2-mm diameter) circular cranial window was drilled in the skull above the somatosensory cortex. Approximately 150 μL of a 3-mg/mL solution of FITC-dextran (molecular mass, 2,000 kDa) in saline was systemically administered via intravascular injection into the retroorbital sinus to enable visualization of the cerebral vasculature and contrast imaging of RBCs. Upon conclusion of surgery, isoflurane anesthesia was replaced with α-chloralose (50 mg/kg) and urethane (750 mg/kg). Body temperature was maintained at 37 °C throughout the experiment using an electric heating pad. Penetrating arterioles were first identified by observing RBCs flowing into the brain (as opposed to out of the brain via venules), and capillaries downstream of arterioles were selected for study. A pipette was next introduced into the solution covering the exposed cortex, and the duration and pressure of ejection were calibrated (300 ms, ~8 to 10 psi) to obtain a small solution plume (radius, ~10 μm). The pipette was maneuvered into the cortex and positioned adjacent to the capillary under study (mean depth, ~73 μm), after which agents were ejected directly onto the capillary. Placement of the pipette in the brain as described restricted agent delivery to the capillary under study and caused minimal displacement of the surrounding tissue. Spatial coverage of the ejected solution was monitored by including 0.06 mg/mL tetramethylrhodamine isothiocyanate (TRITC; 150 kDa)-labeled dextran. RBC flux data were collected by line-scanning the capillary of interest at 5 kHz. Images were acquired using a Zeiss LSM-7 multiphoton microscope (Zeiss) equipped with a Zeiss 20× Plan Apochromat 1.0 N.A. DIC VIS-IR water-immersion objective and coupled to a Coherent Chameleon Vision II Titanium-Sapphire pulsed infrared laser (Coherent). FITC and TRITC were excited at 820 nm, and emitted fluorescence was separated through 500- to 550-nm and 570- to 610-nm bandpass filters, respectively.

1. Blinder P, et al. (2013) The cortical angiome: An interconnected vascular network with noncolumnar patterns of blood flow. *Nat Neurosci* 16:889–897.
2. Shih AY, et al. (2015) Robust and fragile aspects of cortical blood flow in relation to the underlying angioarchitecture. *Microcirculation* 22:204–218.
3. Longden TA, et al. (2017) Capillary K$^+$-sensing initiates retrograde hyperpolarization to increase local cerebral blood flow. *Nat Neurosci* 20:717–726.
4. Longden TA, Nelson MT (2015) Vascular inward rectifier K$^+$ channels as external K$^+$ sensors in the control of cerebral blood flow. *Microcirculation* 22:183–196.
5. Lacroix A, et al. (2015) COX-2-derived prostaglandin E2 produced by pyramidal neurons contributes to neurovascular coupling in the rodent cerebral cortex. *J Neurosci* 35:11791–11810.
6. Zonta M, et al. (2003) Neuron-to-astrocyte signaling is central to the dynamic control of brain microcirculation. *Nat Neurosci* 6:43–50.
7. Wells JA, et al. (2015) A critical role for purinergic signalling in the mechanisms underlying generation of BOLD fMRI responses. *J Neurosci* 35:5284–5292.
8. Kisler K, Nelson AR, Montagne A, Zlokovic BV (2017) Cerebral blood flow regulation and neurovascular dysfunction in Alzheimer disease. *Nat Rev Neurosci* 18:419–434.
9. Dickson EJ, Falkenburger BH, Hille B (2013) Quantitative properties and receptor reserve of the IP$_3$ and calcium branch of G$_q$-coupled receptor signaling. *J Gen Physiol* 141:521–535.
10. Falkenburger BH, Dickson EJ, Hille B (2013) Quantitative properties and receptor reserve of the DAG and PKC branch of G$_q$-coupled receptor signaling. *J Gen Physiol* 141:537–555.
11. Logothetis DE, et al. (2015) Phosphoinositide control of membrane protein function: A frontier led by studies on ion channels. *Annu Rev Physiol* 77:81–104.
12. Huang C-L, Feng S, Hilgemann DW (1998) Direct activation of inward rectifier potassium channels by PIP$_2$ and its stabilization by G$_{\beta\gamma}$. *Nature* 391:803–806.
13. Hille B, Dickson EJ, Kruse M, Vivas O, Suh B-C (2015) Phosphoinositides regulate ion channels. *Biochim Biophys Acta* 1851:844–856.
14. Shyng SL, Nichols CG (1998) Membrane phospholipid control of nucleotide sensitivity of K$_{ATP}$ channels. *Science* 282:1138–1141.
15. Runnels LW, Yue L, Clapham DE (2002) The TRPM7 channel is inactivated by PIP$_2$ hydrolysis. *Nat Cell Biol* 4:329–336.
16. D'Avanzo N, Cheng WWL, Doyle DA, Nichols CG (2010) Direct and specific activation of human inward rectifier K$^+$ channels by membrane phosphatidylinositol 4,5-bisphosphate. *J Biol Chem* 285:37129–37132.
17. Hansen SB, Tao X, MacKinnon R (2011) Structural basis of PIP$_2$ activation of the classical inward rectifier K$^+$ channel Kir2.2. *Nature* 477:495–498.
18. Soom M, et al. (2001) Multiple PIP$_2$ binding sites in Kir2.1 inwardly rectifying potassium channels. *FEBS Lett* 490:49–53.
19. Lopes CMB, et al. (2002) Alterations in conserved Kir channel-PIP$_2$ interactions underlie channelopathies. *Neuron* 34:933–944.
20. Quayle JM, McCarron JG, Brayden JE, Nelson MT (1993) Inward rectifier K$^+$ currents in smooth muscle cells from rat resistance-sized cerebral arteries. *Am J Physiol* 265:C1363–C1370.
21. Hibino H, et al. (2010) Inwardly rectifying potassium channels: Their structure, function, and physiological roles. *Physiol Rev* 90:291–366.
22. Zaritsky JJ, Eckman DM, Wellman GC, Nelson MT, Schwarz TL (2000) Targeted disruption of Kir2.1 and Kir2.2 genes reveals the essential role of the inwardly rectifying K$^+$ current in K$^+$-mediated vasodilation. *Circ Res* 87:160–166.
23. Knight ZA, Shokat KM (2005) Features of selective kinase inhibitors. *Chem Biol* 12:621–637.
24. Hilgemann DW (1997) Cytoplasmic ATP-dependent regulation of ion transporters and channels: Mechanisms and messengers. *Annu Rev Physiol* 59:193–220.
25. Suer S, Sickmann A, Meyer HE, Herberg FW, Heilmeyer LM, Jr (2001) Human phosphatidylinositol 4-kinase isoform PI4K92. Expression of the recombinant enzyme and determination of multiple phosphorylation sites. *Eur J Biochem* 268:2099–2106.
26. Balla A, Balla T (2006) Phosphatidylinositol 4-kinases: Old enzymes with emerging functions. *Trends Cell Biol* 16:351–361.
27. Gehrmann T, et al. (1999) Functional expression and characterisation of a new human phosphatidylinositol 4-kinase PI4K230. *Biochim Biophys Acta* 1437:341–356.
28. Uekawa K, et al. (2016) Obligatory role of EP1 receptors in the increase in cerebral blood flow produced by hypercapnia in the mice. *PLoS One* 11:e0163329.
29. Dabertrand F, et al. (2013) Prostaglandin E$_2$, a postulated astrocyte-derived neurovascular coupling agent, constricts rather than dilates parenchymal arterioles. *J Cereb Blood Flow Metab* 33:479–482.
30. Du X, et al. (2004) Characteristic interactions with phosphatidylinositol 4,5-bisphosphate determine regulation of kir channels by diverse modulators. *J Biol Chem* 279:37271–37281.
31. Kruse M, Hammond GRV, Hille B (2012) Regulation of voltage-gated potassium channels by PI(4,5)P$_2$. *J Gen Physiol* 140:189–205.
32. McNeish AJ, Dora KA, Garland CJ (2005) Possible role for K$^+$ in endothelium-derived hyperpolarizing factor-linked dilatation in rat middle cerebral artery. *Stroke* 36:1526–1532.
33. Jung S-R, et al. (2016) Contributions of protein kinases and β-arrestin to termination of protease-activated receptor 2 signaling. *J Gen Physiol* 147:255–271.
34. Cho H, Lee D, Lee SH, Ho W-K (2005) Receptor-induced depletion of phosphatidylinositol 4,5-bisphosphate inhibits inwardly rectifying K$^+$ channels in a receptor-specific manner. *Proc Natl Acad Sci USA* 102:4643–4648.
35. Cho H, et al. (2005) Low mobility of phosphatidylinositol 4,5-bisphosphate underlies receptor specificity of Gq-mediated ion channel regulation in atrial myocytes. *Proc Natl Acad Sci USA* 102:15241–15246.
36. Jones SA, et al. (1993) PGE2 in the perinatal brain: Local synthesis and transfer across the blood brain barrier. *J Lipid Mediat* 6:487–492.
37. Schmidley JW, Dadson J, Iyer RS, Salomon RG (1992) Brain tissue injury and blood-brain barrier opening induced by injection of LGE$_2$ or PGE$_2$. *Prostaglandins Leukot Essent Fatty Acids* 47:105–110.
38. Wilhelms DB, et al. (2014) Deletion of prostaglandin E$_2$ synthesizing enzymes in brain endothelial cells attenuates inflammatory fever. *J Neurosci* 34:11684–11690.
39. Saper CB (1998) Neurobiological basis of fever. *Ann N Y Acad Sci* 856:90–94.
40. Nakanishi M, Rosenberg DW (2013) Multifaceted roles of PGE$_2$ in inflammation and cancer. *Semin Immunopathol* 35:123–137.
41. Ellis EF, Wei EP, Kontos HA (1979) Vasodilation of cat cerebral arterioles by prostaglandins D$_2$, E$_2$, G$_2$, and I$_2$. *Am J Physiol* 237:H381–H385.
42. Takano T, et al. (2006) Astrocyte-mediated control of cerebral blood flow. *Nat Neurosci* 9:260–267.
43. Aubineau P, Sercombe R, Seylaz J (1980) Parasympathomimetic influence of carbachol on local cerebral blood flow in the rabbit by a direct vasodilator action and an inhibition of the sympathetic-mediated vasoconstriction. *Br J Pharmacol* 68:449–459.
44. Kobrinsky E, Mirshahi T, Zhang H, Jin T, Logothetis DE (2000) Receptor-mediated hydrolysis of plasma membrane messenger PIP$_2$ leads to K$^+$-current desensitization. *Nat Cell Biol* 2:507–514.
45. D'Avanzo N, Lee S-J, Cheng WWL, Nichols CG (2013) Energetics and location of phosphoinositide binding in human Kir2.1 channels. *J Biol Chem* 288:16726–16737.
46. Kawauchi S, et al. (2009) Light scattering change precedes loss of cerebral adenosine triphosphate in a rat global ischemic brain model. *Neurosci Lett* 459:152–156.
47. Matsunaga A, et al. (1998) Energy-dependent redox state of heme a + a$_3$ and copper of cytochrome oxidase in perfused rat brain in situ. *Am J Physiol* 275:C1022–C1030.
48. Ayata C, Lauritzen M (2015) Spreading depression, spreading depolarizations, and the cerebral vasculature. *Physiol Rev* 95:953–993.

PHYSIOLOGY